

# Tuning the Topography of Non-Wetting Surfaces to Reduce Short-Term Microbial Contamination Within Hospitals

Desmond van den Berg, Dalal Asker, Jungchul Kim, Ho-Young Kim, Joanna Aizenberg, and Benjamin Hatton\*

Microbial contamination of hospital surfaces is a major contributor to infectious disease transmission. This work demonstrates that superhydrophobic (Cassie-Baxter) micro post topographies can significantly reduce cell attachment compared to flat controls. For ordered micro post arrays (post diameters 0.3 to 150  $\mu\text{m}$ ), the attachment of four pathogens (*Pseudomonas aeruginosa*, *Staphylococcus aureus*, *Escherichia coli*, and *Candida albicans*) from discrete contaminant droplets upon short-term contact (15 s to 30 min) are assessed. There is a 3-4-log decrease in microbial attachment when reducing the micro posts diameters from 150 to 0.3  $\mu\text{m}$  for all strains, with large posts ( $>20 \mu\text{m}$ ) exhibiting similar attachment rates to flat controls. The critical, maximum feature size to prevent attachment can be tuned depending on the ratio of the cell size to post diameter. Two potential mechanisms are discussed for this size effect. First, application of the random sequential adsorption model shows that this relative post/cell size effect may be due to a reduced probability of attachment, which is theorized to be the dominant mechanism. Alternatively, a physical model is suggested for bacterial cell “pull-off” due to surface tension forces during droplet dewetting. This work may be important for the design of non-wetting antimicrobial surfaces within healthcare environments.

concerned; and after this has been done, our efforts must be directed to the prevention of the entrance of others into it.”<sup>[1]</sup> Lister was the first to recognize the critical need for surgical instrument disinfection, handwashing, and limiting further surface contamination by “germs” within hospitals.

Today, hospital-acquired infections (HAIs) remain a serious problem. HAIs affect 1 in 20 patients and represent  $\approx 10\%$  of total inpatient costs at a burden of an estimated \$35 billion to global health systems.<sup>[2-4]</sup> HAIs can manifest initially as a site-specific infection or respiratory event, then develop into pneumonia and/or sepsis, significantly increasing patient morbidity and mortality.<sup>[5,6]</sup> Common opportunistic pathogens within hospitals associated with HAIs include *Enterococcus faecium*, *Staphylococcus aureus*, *Klebsiella pneumoniae*, *Acinetobacter baumannii*, *P. aeruginosa*, and the *Enterobacter* strains, many of which have acquired drug resistance through the overuse or misuse of antibiotics.<sup>[7-9]</sup>

## 1. Introduction

In 1867 Joseph Lister (“father of modern surgery”) wrote, “Admitting, then, the truth of the germ theory, and proceeding in accordance with it, we must...destroy in the first instance once for all any septic organisms which may exist within the part

Pathogenic transmission within hospitals occurs through aerosolized droplets (respiratory inhalation) and/or touch contact interactions with microbial “reservoir” surfaces known as fomites.<sup>[10-12]</sup> Fomite-person interactions can include patient care, surgical events, and the handling of medical equipment (bedside monitors, handrails, implanted devices).<sup>[11-13]</sup> Microbial

D. van den Berg, D. Asker, B. Hatton  
Department of Materials Science and Engineering  
University of Toronto  
184 College Street, Toronto, Ontario M5S 3E4, Canada  
E-mail: [benjamin.hatton@utoronto.ca](mailto:benjamin.hatton@utoronto.ca)

D. van den Berg, B. Hatton  
Institute of Biomedical Engineering  
University of Toronto  
164 College Street, Toronto, Ontario M5S3G9, Canada

 The ORCID identification number(s) for the author(s) of this article can be found under <https://doi.org/10.1002/adfm.202315957>

© 2024 The Authors. Advanced Functional Materials published by Wiley-VCH GmbH. This is an open access article under the terms of the [Creative Commons Attribution](https://creativecommons.org/licenses/by/4.0/) License, which permits use, distribution and reproduction in any medium, provided the original work is properly cited.

DOI: 10.1002/adfm.202315957

D. Asker  
Food Science & Technology Department  
Alexandria University  
Alexandria 21545, Egypt

J. Kim  
Heat Pump Research Center  
Korea Institute of Machinery & Materials  
156 Gajeongbuk-Ro, Yuseong-Gu, Daejeon 34103, South Korea

H.-Y. Kim  
Department of Mechanical Engineering  
Seoul National University  
1 Gwanak-ro, Gwanak-gu, Seoul 08826, South Korea

J. Aizenberg  
School of Engineering and Applied Sciences and Department of Chemistry and Chemical Biology  
Harvard University  
29 Oxford Street, Cambridge, Massachusetts 02138, USA

transfer to fomites occurs through contaminated droplet contact, settled aerosols, or direct physical touch (Figure 1A,B).<sup>[14–16]</sup> Despite rigorous decontamination protocols, numerous microorganisms can persist on surfaces for days to months; for example, methicillin-resistant *S. aureus* (MRSA) can be viable for months on typical surfaces.<sup>[17–19]</sup>

As Lister foresaw, reducing microbial attachment to fomites is associated with reducing rates of infectious disease.<sup>[20]</sup> A common antimicrobial material design includes enabling biocidal activity, typically by loading materials with antimicrobial agents such as Ag, Cu, chlorohexidine, or essential oils.<sup>[21–23]</sup> However, the time required for diffusional release of antimicrobials can be on the order of hours, while touch contact and pathogen transfer events occur within seconds.<sup>[23–26]</sup> Additional problems are the accumulation of biomass/debris, toxicity concerns, and antimicrobial resistance.<sup>[23,26,27]</sup>

An alternative approach is to prevent the initial microbial attachment altogether through anti-bioadhesive surface designs.<sup>[28]</sup> Examples include polyethylene glycol (PEG), zwitterions, “Slippery Liquid Infused Porous Surfaces” (SLIPS), and polyacrylates.<sup>[29,30]</sup> Although effective in “wet” (implanted device) environments, their applications for “dry” fomite surfaces in hospitals are not feasible; hospital bed rails and touch surfaces cannot be slippery.

There has also been interest in using non-wetting, superhydrophobic surfaces (SHSs) to prevent microbial attachment by limiting the available surface contact area. SHSs are hydrophobic, rough surface topographies that keep fluids in the “Cassie-Baxter” (C-B) wetting state and only allow liquid contact to the micro post tips (Figure 1D,i).<sup>[31,32]</sup> Examples in nature include the self-cleaning property of various plant leaves (‘lotus effect’) in which particulates (dust, parasites) are removed from the leaf surface by mobile water droplets.<sup>[33,34]</sup> However, previous studies aimed at mimicking this self-cleaning effect to produce SHSs to prevent microbial growth have shown limited success.<sup>[35–40]</sup> One challenge is C-B instability, as the sustained water pressure during immersed microbial culture causes a transition to the fully-wetting Wenzel state, also enabled by defects.<sup>[41,42]</sup> In sticky Wenzel conditions, bacteria typically grow very well on and within the rough micro-topographies (Figure 1D,ii). With this C-B instability in mind, we suggest that C-B surfaces are best for preventing microbial attachment in situations involving limited contact with discrete contaminant droplets (i.e., non-immersed conditions). In other words, using SHSs to limit microbial attachment in short-term contamination conditions, not for long-term biofilm growth.

SHSs can be fabricated by etching, photo- or soft lithography<sup>[35–37,43]</sup> for topographies with a wide range of morphology, size, scale, and disorder.<sup>[35,36,44–46]</sup> Previous studies on SHSs to prevent bacterial growth have mostly focused on using either large SHS features (>10 μm),<sup>[38,39]</sup> disordered surfaces,<sup>[35,36,40]</sup> and/or specifically focus on longer-term biofilm growth (typically hours to days),<sup>[36–39]</sup> in which case the transition from a C-B to Wenzel state is inevitable. Certain SHSs have also incorporated biocidal chemistries.<sup>[47]</sup>

The tips of C-B surface features are essentially “islands” that define the available surface for cell attachment,<sup>[48]</sup> as only the tips are in contact with liquid. But there is limited understanding of the role of C-B feature size on self-cleaning or micro-

bial attachment. Experiments with wetting nanotopographies have helped to define the minimum area for bacterial surface attachment,<sup>[46,49,50]</sup> therefore we should expect the diameter of SHS microposts to also be important. Encinas et al. found that *E. coli* biofilm formation (CFU counts, 1 week culture) was reduced by 0.3-log when decreasing SHS (SU-8) micropost diameter from 13 to 5 μm, and a further ≈2-log reduction for a disordered silicone nano-fiber surface.<sup>[38]</sup> However, they did not confirm if the surfaces were still C-B (unlikely after 1 week), and did not report any cytotoxicity testing.

Here we have used uniform micro post arrays to test the influence of SHS feature size on microbial cell attachment by systematically varying the post diameter from “well below” to “well above” the microbial cell size for four different pathogens. Uniform post arrays can teach us much more than disordered, heterogeneous SHSs, which can have drastically varying feature sizes and rates of localized microbial attachment. The micro post diameters were varied from 0.3 μm (smaller than microbial cell size) to 150 μm (significantly larger than microbial cell size) with an overall area fraction of ≈20% (Figure 1E). We measured microbial attachment to the C-B surface after exposure to “contaminated” droplets for contacts of 15 sec to 30 min (Figure 1D). These short times reflect common conditions for droplet contamination of hospital fomites (Figure 1A). We tested four common nosocomial pathogens: a fungus (*C. albicans*), Gram-negative (*P. aeruginosa* PAO1, *E. coli*), and Gram-positive (*S. aureus*) bacteria (Figure 1C).

We demonstrate that microbial cell attachment shows clear trends with respect to micro post diameter and is reduced by several orders of magnitude for micro-posts smaller than the microbial cell size (≤ 1.5 μm), compared to “large” posts or flat surfaces. In fact, for posts > 20 μm, much larger than the microorganisms, we found the attachment is comparable to the flat control samples. This work provides important insights into the optimal design of SHS surfaces to reduce infectious disease transmission due to contaminated droplet contact in hospital environments such as surgical wards.

## 2. Microbial Attachment to Micropost Topographies

All the micro post arrays (Figure 1F) exhibited stable C-B state wettability, which relegates microbial attachment to only the post tips. The static contact angles increased (from 123 ± 3° to 162 ± 2°) with decreasing post size, as expected.<sup>[32]</sup> We measured the transfer of the microbial cells from the contaminated droplets (30 μL) to the test samples, after the 5 min contact time and droplet removal (Figure 1D). The microbial strains range in both cell size and shape (Figure 1C): *C. albicans* is an ovular yeast ≈5 μm in length (and hyphae/daughter cells ≈2 μm); *E. coli* is rod-shaped ≈2 μm in length; *P. aeruginosa* is rod-shaped 2–3 μm in length; and *S. aureus* is spherical (cocci) ≈0.5 μm in diameter.

Figures 2 and 3 show the specific cell counts (# mm<sup>-2</sup>) and fluorescence imaging, respectively, for cells remaining on the micro post samples after droplet removal. Cells (Sytox Green stain) are apparent only on the post tips (none found between posts), confirming that the C-B state was maintained for these droplets.

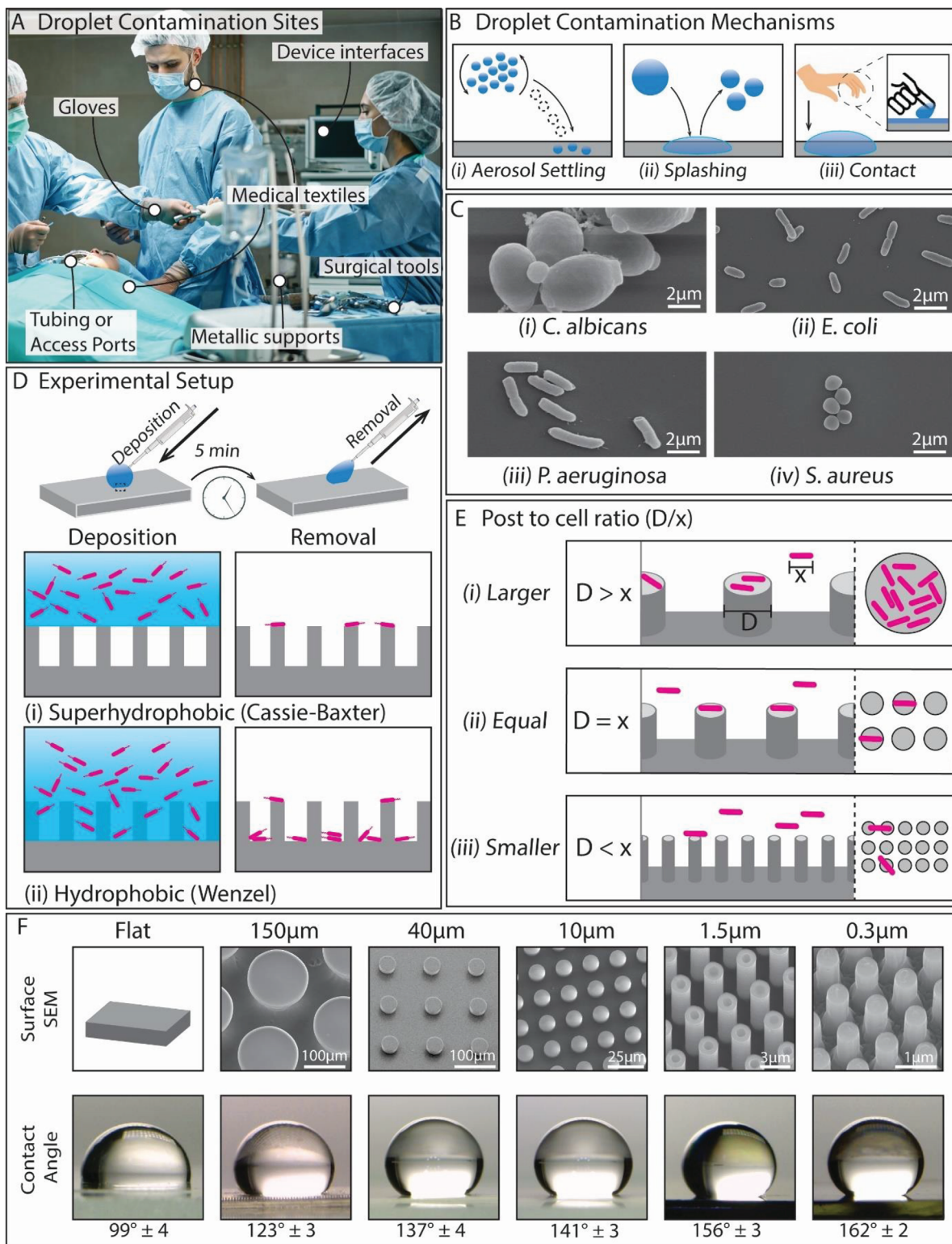


**Figure 1.** A) Examples of sites for contaminated droplet contact with fomite surfaces within a surgical environment and B) the methods by which droplets will propagate (right); C) SEM images of the tested pathogens of varying shape and size; D) Short-term droplet contact experiments by depositing contaminated droplets and removing them after 5 min surface contact. The Cassie-Baxter (C-B) state limits microbial attachment to the post tips (unlike the Wenzel state); E) Nano- and microposts of varying diameters to explore size-dependence of attachment for relative post diameter to cell ratios ( $D/x$ ); F) Examples of micropost arrays and associated contact angles  $\pm$  SD ( $n = 10$ ). Image in panel (A) reproduced under terms of the CC-BY license of Pexels.com.

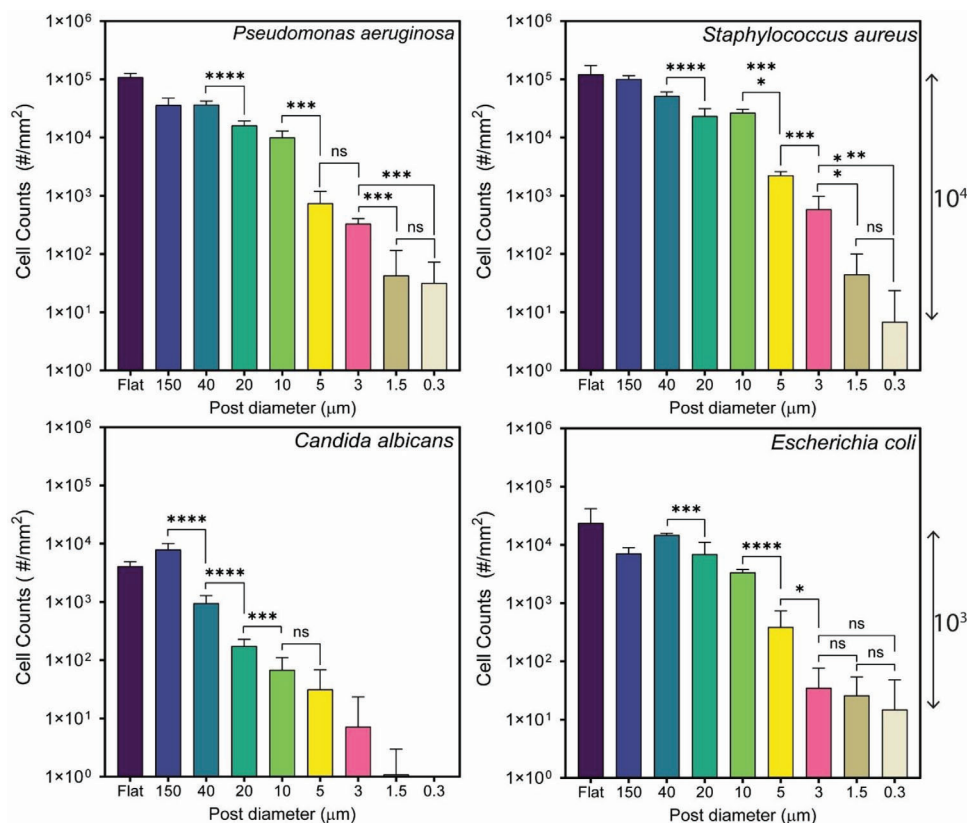


**Figure 2.** Microbial cell counts per  $\text{mm}^2$  (fluorescence microscopy,  $n = 10$ ) as a function of micropost diameter, for all microbial species tested, after droplet contact onto the sample surfaces for 5 min. Significance was calculated using paired two-tailed  $t$ -tests with significance values as stated in the methods section.

These results collectively show that: 1) large-diameter posts behave very similarly to flat surfaces, and 2) there is a significant effect of cell/post size ratio to determine whether cells can attach to the micro-posts.

When reducing the micro post diameter from 150 to 0.3  $\mu\text{m}$ , microbial attachment is reduced drastically by 3 to 4-log (ie; a factor of  $10^3$  to  $10^4$ ). Specifically, there are reductions of 4.25-log (*S. aureus*), 3.53-log (*P. aeruginosa*), 3.20-log (*E. coli*), and 3.58-log (*C. albicans*), when comparing the 150  $\mu\text{m}$  to the 0.3  $\mu\text{m}$  surfaces. Based on these results, the diameters can be grouped as “too large” (>20  $\mu\text{m}$ ), where no significant reduction compared to a flat control exists, or “intermediate” where a steady reduction is observed with decreasing post diameters (10 to 0.3  $\mu\text{m}$ ). Further, cells attached to the post diameters on the order of or smaller than the cells (1.5 and 0.3  $\mu\text{m}$ ) were often found to be located at defect sites, where posts became clumped together (see Figure S1, Supporting Information).

Interestingly, the “too large” micro post surfaces did not result in a significant reduction (higher than 1-log) in attached cells compared to flat controls. Microbial attachment to these surfaces is assumed to be kinetically limited as a result, since the large posts reduced the available surface area by  $\approx 80\%$  but did not lead to a significant reduction in cell counts. It is also worth noting that if the post spacing is on the order of the size of the contaminant, cells may bridge the space between the posts. This result was confirmed by exposing *C. albicans* to a 10  $\mu\text{m}$  post surface

with a 5  $\mu\text{m}$  post spacing, where the larger, “mother” cells were sometimes attached to multiple posts (see Figure S2, Supporting Information).

## 2.1. Kinetics of Attachment to Superhydrophobic Topographies

One of the major drawbacks of C-B surfaces is the metastable state and an eventual transition to the Wenzel regime with time. In fact, many microbes generate surfactants, which reduce surface tension<sup>[51]</sup> and enable this transition; keeping superhydrophobic surfaces in a sustained C-B state with bacteria has not been well documented or clear in the literature.

We tested the longer-term stability of the micro post surfaces by keeping the contaminant droplets in contact for up to 30 min. Figure 4 shows the cell attachment to 10  $\mu\text{m}$  posts, for *P. aeruginosa*, *E. coli*, and *S. aureus* from 15 s to 30 min (counted as cells attached within 24 post areas). The rates of cell attachment were initially rapid with single cells or small clusters of cells attaching to the center of each post (Figure 4C). With increasing attachment time, cells accumulated and packed the post area with further cells before approaching a plateau after 10 min (Figure 4B). This behavior correlates well with a Langmuir adsorption-type behavior, modeled by fitting a one-site-specific binding relationship to the attachment data with  $R^2$  values of 0.893, 0.905, and 0.951 for *S. aureus*, *P. aeruginosa*, and *E. coli*, respectively. Langmuir-type

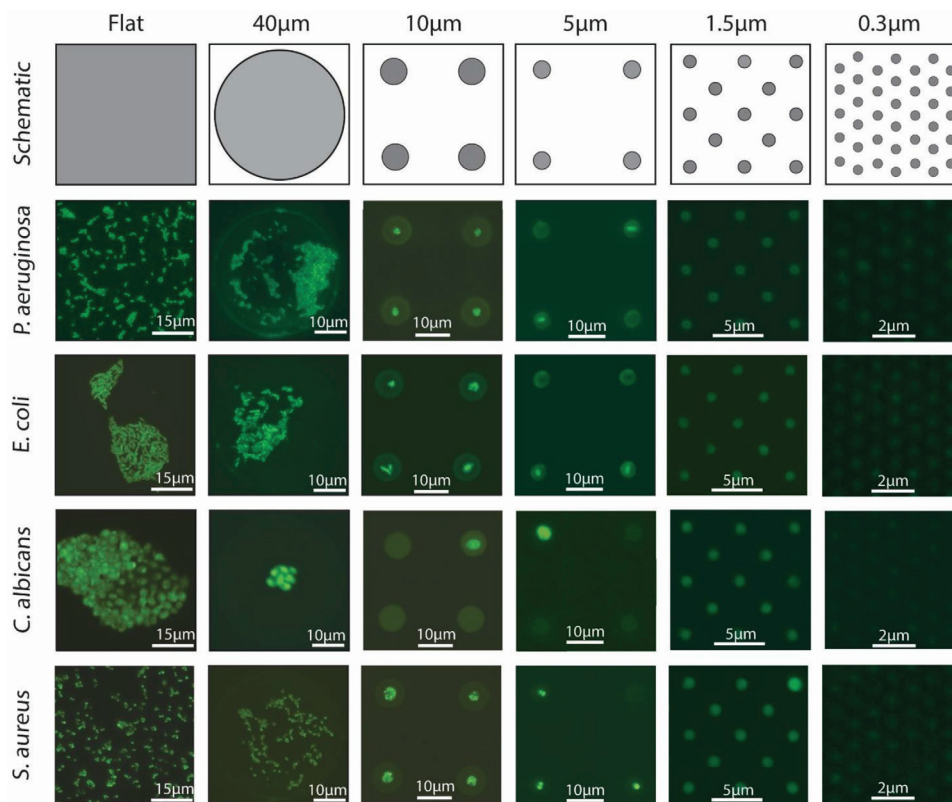


**Figure 3.** Fluorescence microscopy images of the SYTOX-green stained microbial cells remaining on the micro post surfaces after 5 min droplet contact. Microbial cells show as bright green while the post tips themselves also appear fainter, due to adsorption of residual SYTOX-Green stain.

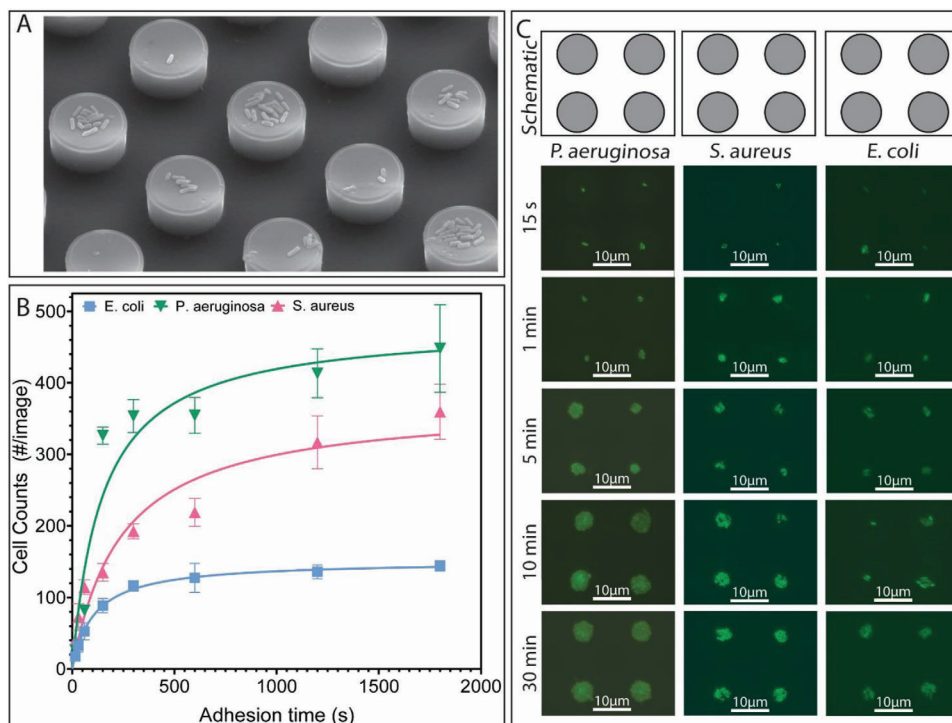


**Figure 4.** (A) SEM image of *P. aeruginosa* on a 10 µm post array after 5 min. (B) Increased bacterial attachment over time, 15 s to 30 min (with average standard deviation) where the y-axis shows attached cells per image area of 24 posts (6 × 4 post area,  $n = 15$ ). (C) Fluorescence images of bacterial accumulation to 10 µm posts with increasing time, showing increasing cell crowding on the post tips.

adsorption has been found previously for bacterial attachment onto standard (full-wetting) surfaces, but this is the first attempt to quantify it for regions of limited area.<sup>[52,53]</sup>

The maximum cell density varied substantially; for example, *E. coli* was 4 times lower than *P. aeruginosa*, which is likely due to strain-specific attachment kinetics. Microbial attachment to surfaces generally occurs in two distinct phases. During initial motility and attachment steps, several reversible attachment steps may be performed until an irreversible attachment event occurs.<sup>[54]</sup> *E. coli* and *P. aeruginosa* both possess pili and flagella which mediate active movement within their suspensions; in comparison, *S. aureus* relies on passive movement within a suspension, with active movement taking place only after colony formation occurs (expressed protein “slime” mediating movement).<sup>[55,56]</sup>

Once near a surface, microbial attachment depends on the interaction of adhesins with surface groups and any conditioning layer, which differs for strains, surface charge, and hydrophobicity.<sup>[56–58]</sup> For example, there is a reduced affinity for *E. coli* to attach to hydrophobic surfaces compared to *P. aeruginosa*, which may explain the reduced overall cell counts for *E. coli*.<sup>[57,59]</sup> Once attached, cell-cell interactions and the recruitment strategies of microbes become important.

## 2.2. Mechanisms of Cell Attachment and Post-Size Effects

We suggest there are two possible mechanisms to explain this significant effect of post size on microbial cell attachment; 1) a “reduced probability of cell attachment” model, and 2) a “cell pull-off” model (Figure 5). The former mechanism focuses on the rates of microbial attachment to the post tips, as circular areas of limited size, and the application of the random sequential adsorption (RSA) model in this context. The latter mechanism focuses on the force balance acting upon each cell by pull-off during droplet de-wetting due to surface tension effects, which also scale with the post size.

### 2.3. The Random Sequential Adsorption (RSA) Model

The Langmuir isotherm-like behavior of Figure 4B,C indicates that the available area for attachment on each post tip decreases with time. One model which can further describe these behaviors is the RSA model. First described as the “parking cars” problem, RSA can describe the rates of particle adsorption to a surface as the size and number of available spaces decreases (as shown in Figure 5A for attachment areas from  $r_1$  to  $r_3$ ).<sup>[60]</sup> The RSA model has been applied previously to particle and protein adsorption as well as bacterial attachment.<sup>[61,62]</sup> We propose that our micro post surfaces, having 2D circular contact areas of different sizes, effectively represent specific “points of time” in this progression of available attachment areas. Thus, the probability of cell attachment to small posts ( $\leq 1.5 \mu\text{m}$ ) should be lower than for larger posts (Figure 5A).

The rate of particle attachment in the RSA model is quantified by the surface coverage function ( $\theta_s$ ) and a blocking potential ( $\beta_1$ ).<sup>[63,64]</sup> The surface coverage function represents the percentage of a surface that contains adsorbed particles, which will

increase with increasing attachment time. Mathematically, this function is represented by:

$$\theta_s = \frac{A_c N_s}{A_p} \quad (1)$$

where  $A_c$  represents the area of the cell (or the projected area occupied by a single cell on a surface),  $A_p$  represents a single micro post area, and  $N_s$  represents the number of attached cells. To calculate the attached cells, the number of cells adsorbed to a single post was measured for 100 post areas. As noted in Figure 4, the surface coverage reaches a plateau after enough time has passed, which is termed the jamming limit of the surface coverage function. For the bacterial species tested, the surface coverage functions are maximized at a value of 0.566 (*S. aureus*) and 0.583 (*E. coli*, *P. aeruginosa*) for areas much larger than the cells.<sup>[62,63]</sup> To assess the influence of post size on this coverage, the post-occupation rate (whether bacteria are present or not, on 100 posts) (Figure 5B,i) was calculated, which showed the initial occupation rates for the small posts was low (1.5–2% for a 1.5  $\mu\text{m}$  post). These rates steadily increased until a plateau of 97–99% was reached for post diameters  $\geq 20 \mu\text{m}$ .

The blocking function (the probability of finding an empty site on a surface) can be calculated through:

$$\beta_1 = \left(1 - \frac{S_e}{A_p}\right)^{N_s} \quad (2)$$

where  $S_e$  is the exclusion area, or the area necessary for a cell to attach. In terms of the total patterned area, all the micro post surfaces generated are effectively “blocked” by 80% (Figure 5A) due to the containment of bacterial attachment to the tips of these posts. Surface blocking functions were calculated by analyzing the area of attached cells compared to the total post area after 5 min contact time. The calculated functions are shown as a function of the micro post diameter (Figure 5B, ii), and show an exponential decay with increasing post diameter. For the rod-shaped bacteria (*E. coli* and *P. aeruginosa*), the blocking functions increased steadily with decreasing diameter, with the steepest transitions occurring between 10–15  $\mu\text{m}$ . For *S. aureus*, this steep transition point occurs between 5–10  $\mu\text{m}$ . For small posts (0.3 or 1.5  $\mu\text{m}$ ), the post tip effectively behaves as a blocked area as noted by the low occupation rates (Figure 5B,i), due to being smaller than the area required for cell attachment. For more information and analysis of the RSA model and fitting to experimental models, refer to Supporting Information Appendix A1.

### 2.4. The Cell “Pull-Off” Model

An alternative mechanism we propose is that cells may have been initially attached to the post tips but were pulled off by surface tension upon droplet removal, considering the force balance acting on a single cell. In this model, cell detachment is achieved if the pull-off force ( $F_p$ ) exerted onto the microbe is larger than the adhesive forces ( $F_A$ ) (Figure 5C). The adhesive forces are a sum of the surface tension effects on the microbe (Laplace pressure and surface tension at the contact line) and the classical physics models for adhesion (van der Waals forces, acid-base interactions, and

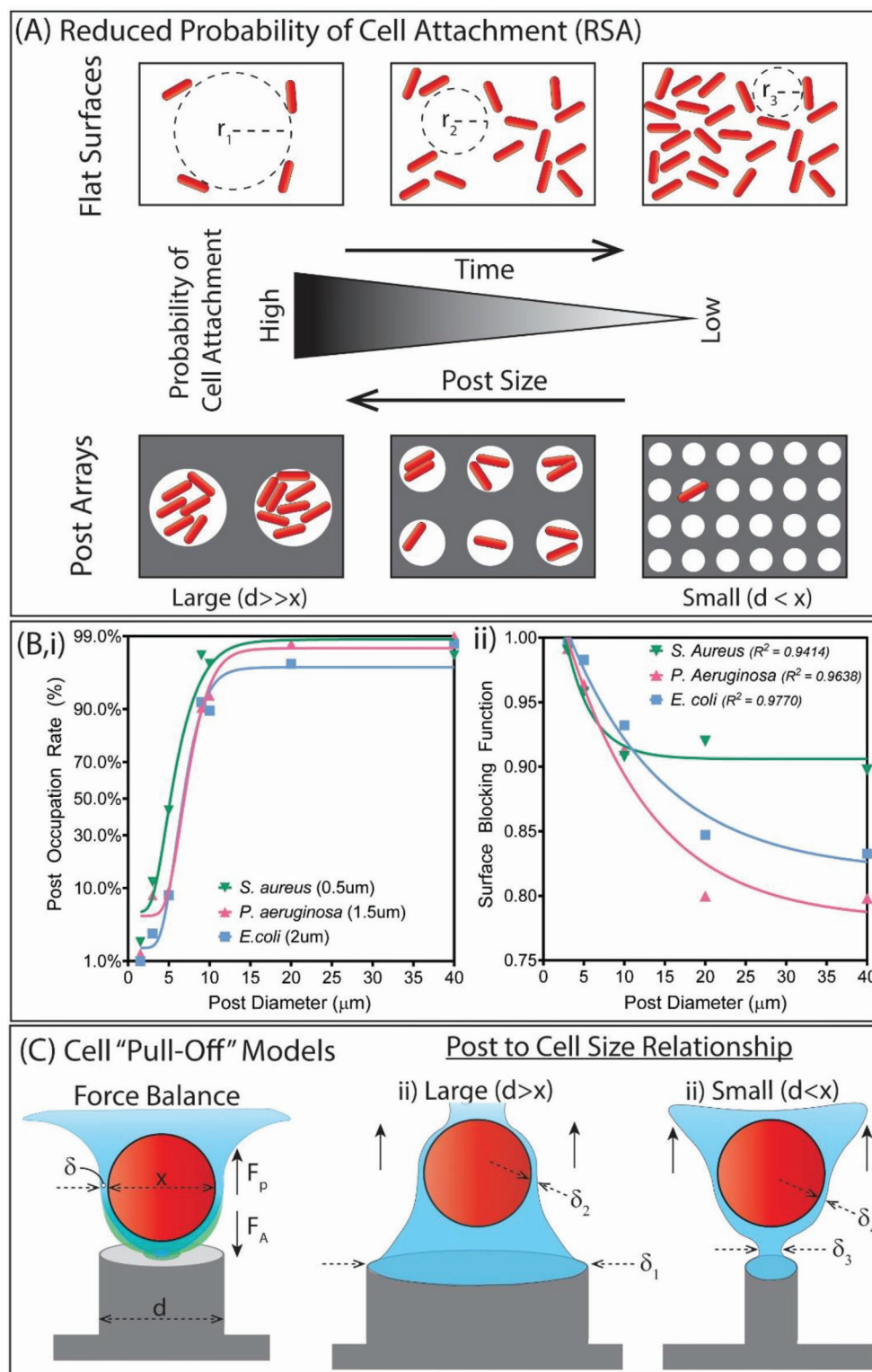


**Figure 5.** Two potential mechanisms are proposed for the “post size” effect on microbial attachment. A) The probability models are explained by considering random sequential adsorption (RSA) and the supporting ideas of excluded/blocked areas and functions B, i) calculations of the post-occupation rate per 100 post area to determine the overall coverage of bacteria after 5 min of contact and ii) calculation of the surface blocking function for each post diameter plotted against post diameter C) cell pull-off models dominated by the attachment and detachment forces with dependence on if the post diameter is smaller or larger than the diameter of a particle.

electrostatics – often referred to as the DLVO or xDLVO model forces).<sup>[65]</sup> The pull-off force, acting in the opposite direction, is due to the surface tension and thickness of the liquid film thickness around the microbe. This thickness and the width of the capillary bridge ( $\delta$ ) will change depending on the diameter of the post ( $d$ ) with respect to the size of the microbe ( $x$ ). Compared to the surface tension force, the van der Waals and electrostatic forces acting on these microbes are much smaller (5–10% of the surface tension), meaning that detachment is favored if possible. It is hypothesized that a post smaller than the microbe may generate a capillary bridge large enough ( $\delta_4 > \delta_3$ ) to overcome these adhesive forces (Figure 5C). More information on this model is provided in Supporting Information Appendix A2.

Both mechanisms may be active under different circumstances depending on the size of the post and droplet contact time. Expansion of the blocking potential functions and surface coverage functions to include the force balance acting upon a particle due to hydrodynamic forces (such as dewetting) can be explored in the future similar to the work of Ko et al.<sup>[66]</sup> In-situ imaging of cell attachment to these surfaces will provide further insights into the likelihood of these distinct mechanisms.

### 3. Discussion

Droplet-based contamination of fomite surfaces represents a common route for infectious disease transmission within hospitals (saliva, blood, wound exudate, etc.), and our work has focused on the short-term contact of such droplets with SHS micro posts. Previous attempts to use SHS topographies to reduce microbial attachment have not been effective, successful, or well-designed for hospital environments, but our work suggests some fundamental reasons, due to feature size and contact time. Our work indicates that previous studies have either used SHS surface features that are too large (and/or heterogeneous feature sizes), or that did not maintain a stable C-B state, or both. In the previous studies cited in the introduction, several used incubation strategies over long periods of time where it becomes difficult to distinguish between wetting versus non-wetting, and between C-B and Wenzel states.

Through the systematic variation of micro post size, for diameters both smaller and larger than microbial cells, and for several microbial strains, we have shown conclusively that this post/size ratio is critical to prevent microbial attachment. The trends associated with microbial cell attachment and micro post size are very clear and show that huge reductions of 3–4-log can be achieved for micro posts of  $\leq 1.5 \mu\text{m}$  diameter compared to posts  $\approx 20 \mu\text{m}$  and flat surfaces. With increasing attachment time, the microbial attachment shows a Langmuir-type isotherm behavior, reaching a plateau after  $\approx 10$  min exposure to  $10 \mu\text{m}$  diameter posts.

We suggest this post/cell size effect for SHS topographies is likely due to a reduced probability of cell attachment to the post-tip areas of limited size (the random sequential adsorption model), as all strains tested show a continuous decrease in attached cell counts for smaller posts. A “threshold” change might suggest the dominance of the “pull off” model. However, both mechanisms may be active to certain extents, with future work centered on the inclusion of hydrodynamic considerations to the RSA model presented similar to that of Ko et al. which evaluated these combined effects for colloidal particle adsorption.<sup>[66]</sup>

This size dependence might suggest that the SHS properties found in a huge diversity of plants and insects ( $>16\,000$  species have been characterized by Barthlott et al.<sup>[67]</sup>) may have topographical features that are evolved for specific pathogens and parasites of specific sizes.<sup>[68,69]</sup> It is important to note that such surfaces in nature are generally not just randomly disordered, but have features (posts, spines, hairs, etc.) in well-defined size ranges, and often sub-micron in scale.

We suggest that certain SHS micro post arrays on hospital fomite surfaces (handrails, fabrics, medical devices) that may contact contaminated droplets for limited times may significantly reduce microbial attachment and further transmission. This work demonstrates important design guidelines for the use of SHS topographies as a promising alternative to existing antimicrobial technologies for fomite surfaces in hospitals. However, there are still considerations to study for the long-term performance of SHSs, such as wear, mechanical damage, and accumulated dust/debris interfering with wettability. In our follow-up work,<sup>[70]</sup> we suggest that medical gloves may represent the ideal application, due to their common use in all short-term touch contact transmission events, and their disposable nature.

### 4. Experimental Section

**Materials:** LB Miller and YPD broths, bacteriological agar, and ethanol were purchased from VWR Canada. Glutaraldehyde (GDA) and Tween-20 were purchased from Sigma Aldrich (Mississauga, ON, Canada). Dymax Light Weld 4–20508 urethane-acrylate blend UV-curable polymer was purchased from Dymax (Torrington, CT, USA). Dow Corning Sylgard 184 silicone elastomer kits were purchased from Paisley Products of Canada Inc. (Scarborough, ON, Canada). SU-8-2025 photoresist was purchased from Kayaku Advanced Materials Inc. (Westborough MA, USA).

**Microbial Species and Their Culture Conditions:** Bacterial cultures of *E. coli* GFP ATCC 25 922, *P. aeruginosa* PAO1, and *S. aureus* KR3 were prepared by obtaining a single colony from a lysogeny broth (LB) Miller agar media plate stock plate which was streaked according to standard methods onto a new plate and incubated overnight at 37 °C. Cultures of *C. albicans* SC5314 were prepared in a similar manner but with yeast extract-peptone-dextrose (YPD).

**Micropost Arrays:** Ordered micro post arrays were fabricated with 0.3, 1.5, 3, 5, 10, 20, and 40  $\mu\text{m}$  diameters (Figure 1E). The micro post arrays were fabricated by photolithography and ion etching, except for the 150  $\mu\text{m}$  post arrays which were purchased commercially (NanogripTech, Setex Technologies, USA). The 0.3 and 1.5  $\mu\text{m}$  post arrays were fabricated using deep reactive ion etching (DRIE), as reported previously.<sup>[48]</sup> All arrays were exposed to oxygen plasma (Harrick Plasma PDC001) for 3 min before fluoro-silanization under vacuum (desiccation chamber and mechanical pump) for 3 h with an open vial containing 50  $\mu\text{L}$  of trichloro (1H, 1H, 2H, 2H-perfluoro octyl) silane (Sigma-Aldrich, Canada) prior to microbial contamination.

**Micropost Array Lithography:** For the 3 to 40  $\mu\text{m}$  diameter samples, Si wafers were cleaned with acetone and covered in 10 mL of SU-8 2025 photoresist. The photoresist was spin-coated (Specialty Coating Systems Model G3P-8) to the desired thickness depending on the diameter of the micro post to be generated. The coated wafer was soft-baked for 30 s at 65 °C and 5 min at 95 °C. A photomask etched under a mask writer (Heidelberg uPG 501) was aligned onto the cooled photoresist wafer and exposed for 18.5 s under a mask aligner (OAI model 30). To complete crosslinking, the wafer was heated for 1 min at 65 °C and 5 min at 95 °C. Sequential submerging and agitation in SU-8 developing solution and isopropyl alcohol followed until all unreacted material was removed from the wafer. Completed master molds exposed to oxygen plasma (Harrick Plasma PDC001) for 3 min before fluoro-silanization under vacuum for 3 h

with an open vial containing 50  $\mu\text{L}$  of trichloro (1H, 1H, 2H, 2H-perfluoro octyl) silane.

Superhydrophobicity of the micropost molds was confirmed by contact angle (DI water) and contact angle hysteresis. Negative molds of the Si micro posts were prepared through soft lithography in polydimethylsiloxane composite (PDMS Sylgard 184). A 10:1 ratio of PDMS composite prepolymer and crosslinker (Dow Corning Sylgard 184) was mixed, degassed, and poured over the wafer before further degassing for 10 min. Curing occurred in a 70  $^{\circ}\text{C}$  oven for 18 h. Completed negative molds were detached after curing from the wafer positives and cleaned with ethanol and DI water.

**UV-Cured Micropost Arrays:** Final micro post arrays were molded by applying 10–20  $\mu\text{L}$  of a UV-curable polyurethane-acrylate (PUA) polymer (Dymax 4–20508) onto a clean glass slide. UV curing through the PDMS mold was performed with a Dymax BlueWave LED DX-1000 Visicure system (405 nm) at full intensity ( $\approx 800 \text{ mW cm}^{-2}$ ) for 200 s. The samples were functionalized with fluorosilane, as described above, to become superhydrophobic. Flat molded PU controls were generated by curing against a flat (as cast) PDMS surface ( $R_a = 0.1 \pm 0.02 \mu\text{m}$ ) as a control.

**Static Contamination Experiments:** The contamination experiments were performed with PUA (Dymax) molds of the 3–40  $\mu\text{m}$  samples, while for the 1.5  $\mu\text{m}$  and 300 nm samples, experiments were performed directly on the Si masters themselves (all treated with the fluorosilane and confirmed to be in the C-B state). Fresh cells were obtained with a sterile loop and suspended in 1X phosphate-buffered saline (PBS) until an optical density ( $\text{OD}_{600}$ ) of  $0.7 \pm 0.05$  for all bacterial strains and  $1.1 \pm 0.05$  for the yeast was obtained as confirmed by UV–vis spectrometry (Cary 60, Aligent Technologies).

A 30  $\mu\text{L}$  suspension droplet was pipetted onto  $1 \times 1 \text{ cm}^2$  micro post samples and left for 5 min before removal by capillary wicking with a Kimwipe tissue or pipet. A 30  $\mu\text{L}$  droplet of 2.5% GDA in 1X PBS was placed over the same contact area for 5 min and was then removed and a droplet of 0.05% Tween-20 in 0.9% NaCl v/v was added. The attached microbes were stained with a 50  $\mu\text{L}$  drop of a Sytox Green solution (1  $\mu\text{L}/10 \text{ mL}$  in 1X PBS) for 10 min. Microbial attachment was assessed through fluorescence microscopy (Olympus BX63, Tokyo, Japan) using a GFP filter ( $\lambda_{\text{ex}}/\lambda_{\text{em}}$  395/470 nm). Image analysis was performed by surveying the array under low magnification and centering into the stained portion to ensure that each image allowed for optimal attachment to the posts contained. These areas were analyzed using Olympus cellSens software.

**Contact Angle Measurements:** A total of 10  $\mu\text{L}$  droplets of DI water were applied to the silanized micro post surfaces to assess the static contact angle using a lab-made goniometer system. Droplet images were analyzed using ImageJ and the contact angle plugin (Marco Brugnara).

**Scanning Electron Microscopy (SEM):** To measure the size of the microbial cells and assess contamination density, 10  $\mu\text{m}$  micro post arrays, and flat control surfaces were prepared for SEM imaging. Fixation procedures described in the static contamination experiments were followed by washing five times with 100  $\mu\text{L}$  of 1X PBS. The samples were dehydrated through sequential ethanol and water mixtures (25, 50, 70, 80, 90, 100% v/v, 15 min each), then critical point dried (Bal-Tec CPD 030 Critical Point Dryer) and Au sputter-coated before SEM (Hitachi SU3500 – Variable Pressure). SEM of each type of microbial cell was obtained by spreading a suspension of the microbial cells onto a silicon wafer and treating them as described above.

**Data and Statistical Analysis:** All experimental counts are plotted as a mean value and an error bar of the standard deviation ( $\pm$ ) using paired, two-tailed *t*-tests as the statistical method to calculate the significance of the reported data. All significant differences plotted in the Figures are – ns ( $p \geq 0.05$ ), \* ( $p$  between 0.01 to 0.05), \*\* ( $p$  between 0.001 to 0.01), \*\*\* ( $p$  between 0.0001 to 0.001), or \*\*\*\* ( $p < 0.0001$ ). All data was processed using GraphPad Prism.

## Supporting Information

Supporting Information is available from the Wiley Online Library or from the author.

## Acknowledgements

The authors acknowledge the help of Lindsey Fiddes with electron microscopy (Medical Sciences, UofT). Funding: Natural Sciences and Engineering Research Council of Canada (NSERC) Discovery grant (RGPIN-2019-06760) (B.D.H.), The Canadian Foundation for Innovation (CFI) #31799 (B.D.H.), the Emerging & Pandemic Infections Consortium (EPIC), UofT (B.D.H) and a Percy Edward Hart Professorship, UofT (B.D.H.).

## Conflict of Interest

The authors declare no conflict of interest.

## Data Availability Statement

The data that support the findings of this study are available from the corresponding author upon reasonable request.

## Keywords

bacterial attachment, fomite, infectious disease transmission, superhydrophobic surfaces

Received: December 13, 2023

Revised: April 2, 2024

Published online: May 1, 2024

- [1] J. Lister, *The Lancet* **1867**, 90, 668.
- [2] R. D. Scott, 2nd, S. D. Culler, K. J. Rask, *J Infus Nurs* **2019**, 42, 61.
- [3] P. W. Stone, *Expert Rev Pharmacoecon Outcomes Res* **2009**, 9, 417.
- [4] A. Marchetti, R. Rossini, *J Med Econ* **2013**, 16, 1399.
- [5] J. Johnstone, G. Garber, M. Muller, *CMAJ* **2019**, 191, E977.
- [6] S. E. Cosgrove, *Clin. Infect. Dis.* **2006**, 42, S82.
- [7] D. M. Costa, K. Johani, D. S. Melo, L. K. O. Lopes, L. K. O. Lopes Lima, A. F. V. Tipple, H. Hu, K. Vickery, *Lett Appl Microbiol* **2019**, 68, 269.
- [8] J. A. Otter, S. Yezli, G. L. French, *Infect Control Hosp Epidemiol* **2011**, 32, 687.
- [9] C. N. I. Surveillance, *Can Commun Dis Rep* **2020**, 46, 99.
- [10] K. Johani, D. Abualsaud, D. M. Costa, H. Hu, G. Whiteley, A. Deva, K. Vickery, *J Infect Public Health* **2018**, 11, 418.
- [11] L. Cobrado, A. Silva-Dias, M. M. Azevedo, A. G. Rodrigues, *Eur J Clin Microbiol Infect Dis* **2017**, 36, 2053.
- [12] D. Pittet, B. Allegranzi, H. Sax, S. Dharan, C. L. Pessoa-Silva, L. Donaldson, J. M. Boyce, *Lancet Infect. Dis.* **2006**, 6, 641.
- [13] A. Wolfensberger, L. Clack, S. P. Kuster, S. Passerini, L. Mody, V. Chopra, J. Mann, H. Sax, *Infect Control Hosp Epidemiol* **2018**, 39, 1093.
- [14] S. M. Kotay, R. M. Donlan, C. Ganim, K. Barry, B. E. Christensen, A. J. Mathers, A. J. McBain, *Appl. Environ. Microbiol.* **2019**, 85, e01997.
- [15] A. J. Prussin 2nd, E. B. Garcia, L. C. Marr, *Environ. Sci. Technol. Lett.* **2015**, 2, 84.
- [16] L. Bourouiba, *Annu. Rev. Fluid Mech.* **2021**, 53, 473.
- [17] K. Vickery, A. Deva, A. Jacombs, J. Allan, P. Valente, I. B. Gosbell, *J Hosp Infect* **2012**, 80, 52.
- [18] B. Hota, *Clin. Infect. Dis.* **2004**, 39, 1182.
- [19] A. Kramer, I. Schwebke, G. Kampf, *BMC Infect. Dis.* **2006**, 6, 130.
- [20] B. Stephens, P. Azimi, M. S. Thoemmes, M. Heidarnejad, J. G. Allen, J. A. Gilbert, *Curr Pollut Rep* **2019**, 5, 198.
- [21] P. N. Danese, *Alkaloids Chem Biol* **2002**, 9, 873.

- [22] H. A. Foster, I. B. Ditta, S. Varghese, A. Steele, *Appl. Microbiol. Biotechnol.* **2011**, *90*, 1847.
- [23] C. Adlhart, J. Verran, N. F. Azevedo, H. Olmez, M. M. Keinänen-Toivola, I. Gouveia, L. F. Melo, F. Crijs, *J. Hosp Infect* **2018**, *99*, 239.
- [24] C. Liao, Y. Li, S. C. Tjong, *Nanomaterials* **2020**, *10*.
- [25] A. Jose, M. Gizdavic-Nikolaidis, S. Swift, *Appl. Microbiol.* **2023**, *3*, 145.
- [26] A. Lansdown, A. Williams, *Nurs Times* **2007**, *103*, 48.
- [27] C. E. Santo, P. V. Morais, G. Grass, *Appl. Environ. Microbiol.* **2010**, *76*, 1341.
- [28] J. Genzer, K. Efimenko, *Biofouling* **2006**, *22*, 339.
- [29] T. S. Wong, S. H. Kang, S. K. Tang, E. J. Smythe, B. D. Hatton, A. Grinthal, J. Aizenberg, *Nature* **2011**, *477*, 443.
- [30] A. M. C. Maan, A. H. Hofman, W. M. de Vos, M. Kamperman, *Adv. Funct. Mater.* **2020**, *30*, 2000936.
- [31] M. Callies, D. Quere, *Soft Matter* **2005**, *1*, 55.
- [32] D. Quere, *Ann. Rev. Mater. Res.* **2008**, *38*, 71.
- [33] W. Barthlott, C. Neinhuis, *Planta* **1997**, *202*, 1.
- [34] K. Koch, W. Barthlott, *Philos. Trans. R. Soc., A* **2009**, *367*, 1487.
- [35] L. R. Freschtauf, J. McLane, H. Sharma, M. Khine, *PLoS One* **2012**, *7*, e40987.
- [36] X. Lan, B. Zhang, J. Wang, X. Fan, J. Zhang, *Colloids Surf. A* **2021**, *624*, 126820.
- [37] S. M. R. Razavi, J. Oh, R. T. Haasch, K. Kim, M. Masoomi, R. Bagheri, J. M. Schlauch, N. Miljkovic, *ACS Sustainable Chem. Eng.* **2019**, *7*, 14509.
- [38] N. Encinas, C.-Y. Yang, F. Geyer, A. Kaltbeitzel, P. Baumli, J. Reinholz, V. Mailänder, H.-J. Butt, D. Vollmer, *ACS Appl. Mater. Interfaces* **2020**, *12*, 21192.
- [39] E. Sadler, A. S. Stephen, R. P. Allaker, C. R. Crick, *Adv. Mater. Interfaces* **2023**, *10*, 2202532.
- [40] X. Zhang, L. Wang, E. Levänen, *RSC Adv.* **2013**, *3*, 12003.
- [41] D. Murakami, H. Jinnai, A. Takahara, *Langmuir* **2014**, *30*, 2061.
- [42] G. B. Hwang, K. Page, A. Patir, S. P. Nair, E. Allan, I. P. Parkin, *ACS Nano* **2018**, *12*, 6050.
- [43] A. Uneputty, A. Dávila-Lezama, D. Garibo, A. Oknianska, N. Bogdanchikova, J. F. Hernández-Sánchez, A. Susarrey-Arce, *Colloid Interface Sci. Commun.* **2022**, *46*, 100560.
- [44] N. Lu, W. Zhang, Y. Weng, X. Chen, Y. Cheng, P. Zhou, *Food Control* **2016**, *68*, 344.
- [45] F. Hizal, C. H. Choi, H. J. Busscher, H. C. van der Mei, *ACS Appl. Mater. Interfaces* **2016**, *8*, 30430.
- [46] T. S. Heckmann, J. D. Schiffman, *ACS Appl. Nano Mater.* **2020**, *3*, 977.
- [47] Y. Zhan, S. Yu, A. Amirfazli, A. Rahim Siddiqui, W. Li, *Adv. Eng. Mater.* **2022**, *24*, 2101053.
- [48] B. D. Hatton, J. Aizenberg, *Nano Lett.* **2012**, *12*, 4551.
- [49] R. S. Friedlander, H. Vlamakis, P. Kim, M. Khan, R. Kolter, J. Aizenberg, *Proc. Natl. Acad. Sci. USA* **2013**, *110*, 5624.
- [50] L. C. Hsu, J. Fang, D. A. Borca-Tasciuc, R. W. Worobo, C. I. Moraru, *Appl. Environ. Microbiol.* **2013**, *79*, 2703.
- [51] M. A. M. Dias, M. Nitschke, *Braz J Microbiol* **2023**, *54*, 103.
- [52] J. Pringle, H. M. F., *Microbiology* **1986**, *132*, 743.
- [53] A. Borkowski, M. Szala, T. Cłapa, *Appl. Biochem. Biotechnol.* **2015**, *175*, 1448.
- [54] M. D. Hoffman, L. I. Zucker, P. J. Brown, D. T. Kysela, Y. V. Brun, S. C. Jacobson, *Anal. Chem.* **2015**, *87*, 12032.
- [55] M. C. Duvernoy, T. Mora, M. Ardre, V. Croquette, D. Bensimon, C. Quilliet, J. M. Ghigo, M. Balland, C. Beloin, S. Lecuyer, N. Desprat, *Nat. Commun.* **2018**, *9*, 1120.
- [56] E. J. G. Pollitt, S. P. Diggle, *Cell. Mol. Life Sci.* **2017**, *74*, 2943.
- [57] J. K. Oh, Y. Yegin, F. Yang, M. Zhang, J. Li, S. Huang, S. V. Verkhoturov, E. A. Schweikert, K. Perez-Lewis, E. A. Scholar, T. M. Taylor, A. Castillo, L. Cisneros-Zevallos, Y. Min, M. Akbulut, *Sci. Rep.* **2018**, *8*, 17247.
- [58] C. Heilmann, in *Bacterial Adhesion: Chemistry, Biology and Physics*, (Eds: D. Linke, A. Goldman), Springer Netherlands, Dordrecht, **2011**, p. 105.
- [59] I. De-la-Pinta, M. Cobos, J. Ibarretxe, E. Montoya, E. Eraso, T. Guraya, G. Quindós, *J. Mater. Sci.: Mater. Med.* **2019**, *30*, 77.
- [60] A. Rényi, *Publ. Math. Inst. Hungar. Acad. Sci.* **1958**, *3*, 109.
- [61] B. M. Manzi, M. Werner, E. P. Ivanova, R. J. Crawford, V. A. Baulin, *Sci. Rep.* **2019**, *9*, 4694.
- [62] A. J. d. Kerchove, M. Elimelech, *Environ. Sci. Technol.* **2008**, *42*, 4371.
- [63] Z. Adamczyk, M. Nattich-Rak, M. Sadowska, A. Michna, K. Szczepaniak, *Colloids Surf. A* **2013**, *439*, 3.
- [64] Z. Adamczyk, P. Weroński, E. Musiał, *J. Colloid Interface Sci.* **2001**, *241*, 63.
- [65] M. Hermansson, *Colloids Surf., B* **1999**, *14*, 105.
- [66] C.-H. Ko, S. Bhattacharjee, M. Elimelech, *J. Colloid Interface Sci.* **2000**, *229*, 554.
- [67] W. Barthlott, M. Mail, C. Neinhuis, *Philos. Trans. R. Soc., A* **2016**, *374*, 20160191.
- [68] A. Tripathy, P. Sen, B. Su, W. H. Briscoe, *Adv. Colloid Interface Sci.* **2017**, *248*, 85.
- [69] G. S. Watson, D. W. Green, L. Schwarzkopf, X. Li, B. W. Cribb, S. Myhra, J. A. Watson, *Acta Biomater.* **2015**, *21*, 109.
- [70] D. van den Berg, D. Asker, E. Sohrmann, B. D. Hatton, Manuscript in preparation **2024**.